Supplementary Information

for

Incorporating spatial heterogeneity into evapotranspiration estimates for bioretention basins

Joshua S. Caplan, Martin Bouda, Allyson B. Salisbury,
Michael Alonzo, Jonathan E. Nyquist, Laura Toran, Sasha W. Eisenman

Supplement 1: Extended Methods

Chamber ET flux measurements

ET measurements were made using the closed dynamic chamber method, in which plots are covered with airtight chambers open only to the soil. Although more commonly used to measure carbon fluxes (e.g., Geoghegan et al., 2018; Norman et al. 1997), the method has been successfully applied to water flux measurement as well (Garcia et al., 2008; Hamel et al., 2015; Luo, 2015). Custom-made collars were set into the soil at the beginning of the field season; collars demarcated plot boundaries (Figure 1). The upper faces of collars were square (52 × 52 cm or 92 × 92 cm) and approximately parallel to the basin's bottom (i.e., not the basins' sloped sides). Small collars were installed at the eight plots with minimal or short-stature vegetation approximately a week before the first measurement campaign while the large collars were installed at the three plots with taller vegetation between the first and second measurement dates. Collar walls were transparent and typically extended 2-6 cm into the soil. Each measurement day, gaps between collar walls and the ground surface were filled with soil to prevent water vapor from entering or escaping during ET measurement. Vegetation that had grown in minimally-vegetated plots was also clipped to within ~0.5 cm of the soil surface at the beginning of each measurement day.

We measured ET at each plot approximately five times per measurement day, typically between 800 and 1900 h at approximately 90-minute intervals. For each measurement, first we placed a transparent chamber onto the abovementioned collar. Chambers were 52 × 52 × 52 cm or 92 × 92 × 62.5 cm; closed-cell foam was attached to the rims of open faces (i.e., at the top and bottom of chambers) so they would form airtight seals. We clamped the collar and transparent chamber together and placed at least one small, battery-powered fan within the chamber to continually mix air. We measured water vapor in the chamber once per second using an ultra-portable greenhouse gas analyzer (UGGR; Los Gatos Research, San Jose, CA, USA) that was connected to the chamber using a pair of flexible tubes (4.3 m long). Data were recorded in units of partial pressure (specifically μmol mol^{-1}, or ppm) for at least 2 min when using small chambers and at least 3 min when using large chambers.

Calculating rates of ET required isolating the linear portions of time series recorded while chambers were closed and performing linear regression analysis with the extracted data. The resulting rates are proportional to ET but reflect changes in water vapor partial pressure (ET_{ppm}) rather than the actual amount of water vapor. Conversion to the quantity of water vapor per time (ET_{mmol}) was made by multiplying regression slopes (in ppm s^{-1}) by the total amount of air in the chamber, collar, and UGGR (n, in mol). The total amount of air in the systems was determined based on the ideal gas law:

$$ET_{mmol} = ET_{ppm} \times n = (P \times V)/(R \times T),$$

where P is the measured partial pressure (in atm), V is the total volume of the enclosed air space (in L), R is the universal gas constant (0.082057 L atm K^{-1} mol^{-1}), and T is the air's temperature (in K). Finally, ET_{mmol} values were normalized to the sampled plot area (A, in m^2), thus yielding fluxes in units of mmol H_2O m^{-2} s^{-1}, and multiplied by a correction factor that accounts for water vapor adsorbing to interior surfaces of tubing (1.187); it was interpolated from values in Hamel et al. (2015) given the length of tubing we used (4.3 m):

$$ET = ET_{mmol} \times 1.187 / A.$$

Basin Spatial Characterization

We characterized the basin's topography and spatial heterogeneity in vegetation height using a combination of terrestrial LiDAR scanning and drone-based photogrammetry. We first used a Trimble TX5 3D terrestrial laser scanner (Trimble Inc., Sunnyvale, CA, USA) to generate a digital elevation model (DEM) of SMP A. The laser scanner was mounted on a tripod and generated point clouds extending up to 60 m from the laser scanner. We performed 13 scans from different positions within the basin to ensure line of sight with the vast majority of the ground surface (i.e., to minimize "shadows" from vegetation and other structures). At least three targets (glass sphere or paper checkerboard) were included in every scan; these used to georeference each XYZ point cloud scan to the others. We further recorded the coordinates of 12 of the target locations using a Trimble GeoXH GPS unit (Trimble Inc., Sunnyvale, CA, USA) and used their coordinates to georeference the point cloud in the universal transverse mercator (UTM) coordinate system. The GPS unit had a 10-cm accuracy after post-processing, though the

laser scanner had an accuracy <1 cm. We merged, georeferenced, and trimmed areas outside of the basin using Trimble RealWorks (Trimble Inc., Sunnyvale, CA, USA). We further refined the dataset by removing points associated with vegetation and manmade structures (e.g., a metal cage around the basin's outlet) using the *lasground_new* algorithm from LAStools (rapidlasso GmbH, Gilching, Germany). We then used an adaptive triangular network algorithm from LAStools to extract the ground surface (Axelsson, 2000). Small areas where the laser could not achieve line of sight were interpolated. Finally, we converted the dataset into a 10-cm gridded raster using Quick Terrain Modeler (Applied Imagery, Chevy Chase, MD, USA).

We generated a digital surface model (DSM) from drone-based photographs using a structure-from-motion approach (following Alonzo et al., 2018). We flew a Phantom 4 Pro drone (DJI Technology, Shenzhen, China) in a manual grid pattern over the basin with an off-nadir camera view to establish convergent view geometry (Alonzo 2020). This process yielded 286 photos with at least 80% front/back overlap and sidelap. The photos were processed to generate a point cloud using Pix4Dmapper 4.6.4 (Pix4D S.A., Prilly, Switzerland). This included manual georeferencing to a set of 5 visible tie points, allowing for co-registration of the final DSM with the DEM described above. From the point cloud, we created and exported a high-resolution orthomosaic and a DSM. Vegetation cover and height were established by subtracting the DEM model results from the structure-from-motion DSM. The DEM and DSM data also enabled us to manually create a set of polygons that demarcated topographic positions within the basin.

Supplement 2: ET Model Variables

Table S1. ET models with the input weather variables and constants used for comparison with simulated ET. All ET models were implemented using the R package *evapotranspiration* (Guo et al., 2016)

Name	**Type**	**Input Variables**	**Constants**	**Source**
Priestly-Taylor	Potential ET	RHmax RHmin Rs Tmax Tmin	αPT Elev G Gsc λ Lat Σ	Priestly & Taylor, 1972
Matt-Shuttleworth	Reference ET	RHmax RHmin Rs Tmax Tmin U2 or Uz	α = 0.23 Ca CH = 0.12 m Elev Gsc λ Lat Roua rs = 70 s m^{-1} σ z	Shuttleworth & Wallace, 2009
Hargreaves	Reference ET	Tmax Tmin	Elev GSc Lambda Lat	Hargreaves & Samani, 1985
Penman-Monteith FAO	Reference ET	RHmax RHmin Rs Tmax Tmin U2 or Uz	α = 0.23 CH = 0.12 m Elev G Gsc λ Lat rs = 70 s m^{-1} σ z	Allen et al., 1998
Penman-Monteith ASCE	Reference ET	RHmax RHmin Rs Tmax Tmin U2 or Uz	α = 0.23 CH = 0.50 m Elev G Gsc λ Lat rs = 45 s m^{-1} σ z	Allen, 2005
Granger-Gray	Actual ET	RHmax RHmin Rs Tmax Tmin U2 or Uz	α = 0.23 Elev G Gsc λ Lat σ z	Granger and Gray, 1989

Abbreviations:

α = albedo of evaporative surface
αPT = Priestly-Taylor coefficient, 1.26
Ca = specific heat of air, 0.001013 MJ kg^{-1} $^oC^{-1}$
CH = crop height
Elev = ground elevation above mean sea level
G = soil heat flux
Gsc = solar constant, 0.0820 MJ m^{-2} min^{-1}
λ = latent heat of vaporization, 2.45 MJ kg^{-1}
Lat = latitude
RHmax = maximum relative humidity
RHmin = minimum relative humidity
Roua = mean air density, 1.20 kg m^{-3}
Rs = solar radiation
rs = surface resistance
σ = Stefan-Boltzmann constant, $4.903*10^{-9}$ MJ K^{-4} m^{-2} day^{-1}
Tmax = maximum temperature
Tmin = minimum temperature
U2 = wind speed at 2 m
Uz = wind speed at height z
z = height of wind instrument

Supplement 3: Empirical ET Model Results

Table S2. Coefficients of the empirical model of ET from closed-chamber water flux measurements. The response variable (ET) was square-root transformed for fitting. Topo = topographic position, where 0 = low and 1 = high; Plant Size = plant height; VPD = vapor pressure deficit; Solar Rad = solar radiation; VWC = volumetric water content

Variable	**β**	χ^2	***p***
Topo	-0.158	1.6	0.200
Plant Size	0.093	8.2	0.004
VPD	0.375	114.6	<0.001
Solar Rad	0.393	247.8	<0.001
VWC	0.060	0.2	0.637
Topo × Plant Size	0.068	0.5	0.464
Topo × VPD	-0.030	0.2	0.639
Topo × Solar Rad	-0.049	1.7	0.198
Topo × VWC	-0.025	0	0.824
Plant Size × VPD	-0.023	0.5	0.481
Plant Size × Solar Rad	0.010	2.7	0.103
Plant Size × VWC	-0.025	3	0.083
VPD × Solar Rad	-0.019	0.3	0.570
VPD × VWC	0.181	25.3	<0.001
Solar Rad × VWC	-0.089	0.5	0.494
Topo × Plant Size × VPD	0.066	1.6	0.212
Topo × Plant Size × Solar Rad	0.072	2.1	0.145
Topo × Plant Size × VWC	-0.054	0.7	0.387
Topo × VPD × Solar Rad	0.029	0.3	0.556
Topo × VPD × VWC	-0.050	0.8	0.382
Topo × Solar Rad × VWC	0.112	5.4	0.020
Plant Size × VPD × Solar Rad	-0.020	0.7	0.405
Plant Size × VPD × VWC	-0.023	0.6	0.445
Plant Size × Solar Rad × VWC	-0.015	0.3	0.561
VPD × Solar Rad × VWC	0.044	1.6	0.213

Supplement 4: Additional Figures

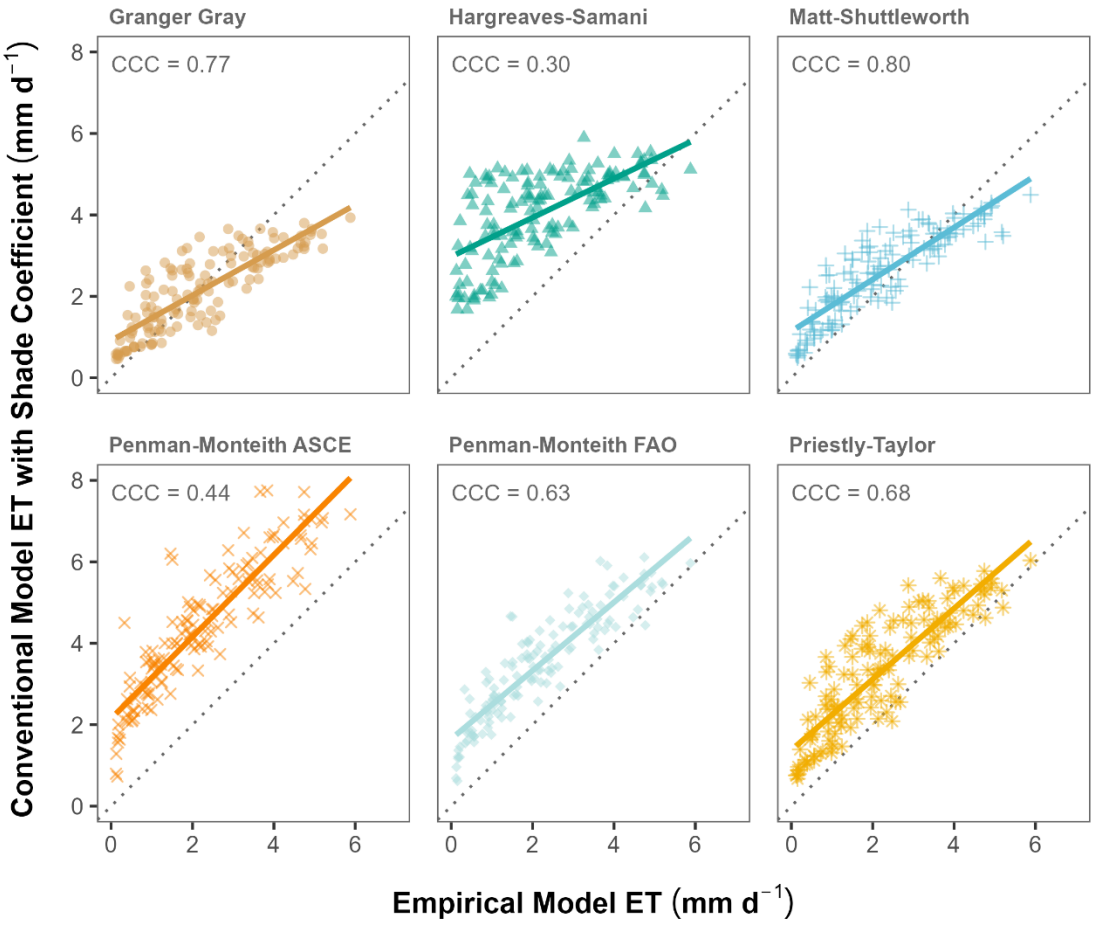

Figure S1: Daily ET calculated from our basin-scale, empirically-based model vs. ET from six conventional models whose solar radiation input data were modified to account for shade from nearby structures. Dotted lines depict 1:1 relationships. CCC = concordance correlation coefficient.

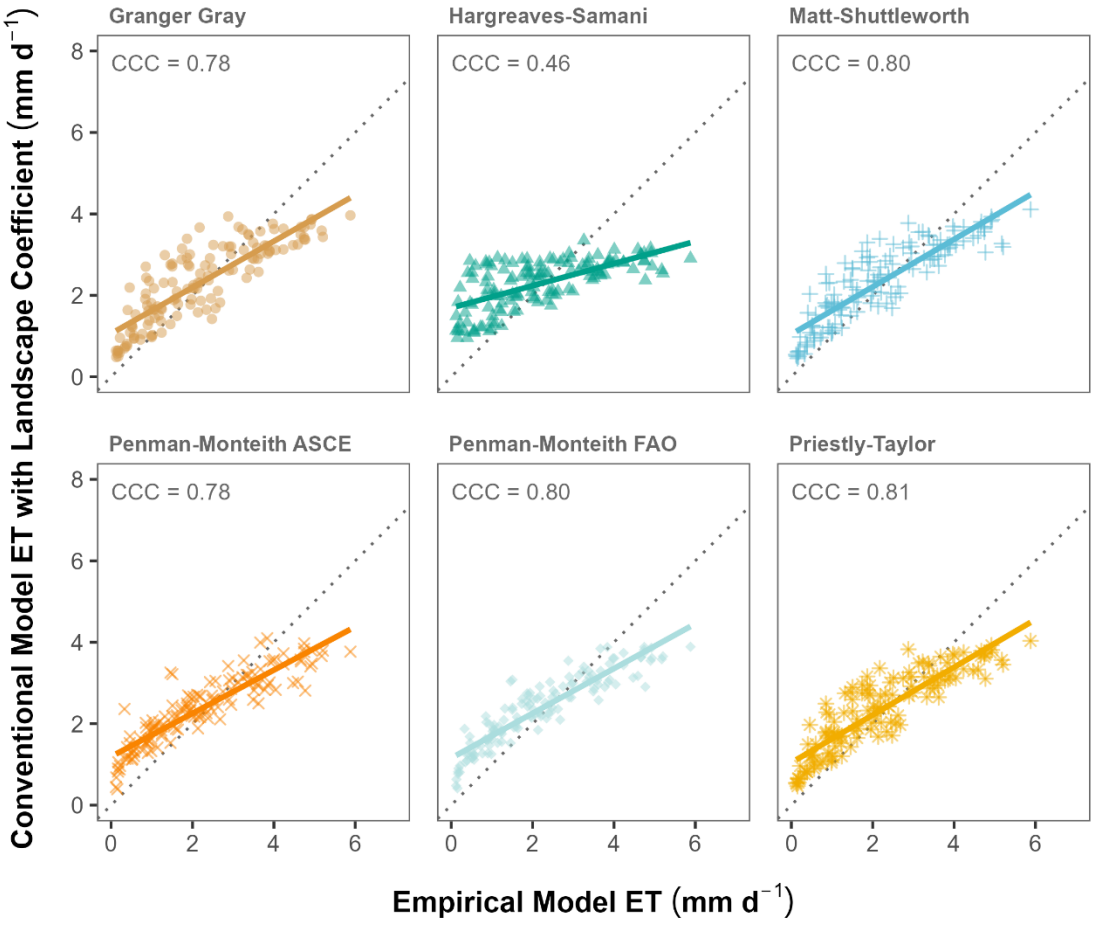

Figure S2: Daily ET calculated from our basin-scale, empirically-based model vs. ET from six conventional models that were modified with a landscape coefficient. Dotted lines depict 1:1 relationships. CCC = concordance correlation coefficient.

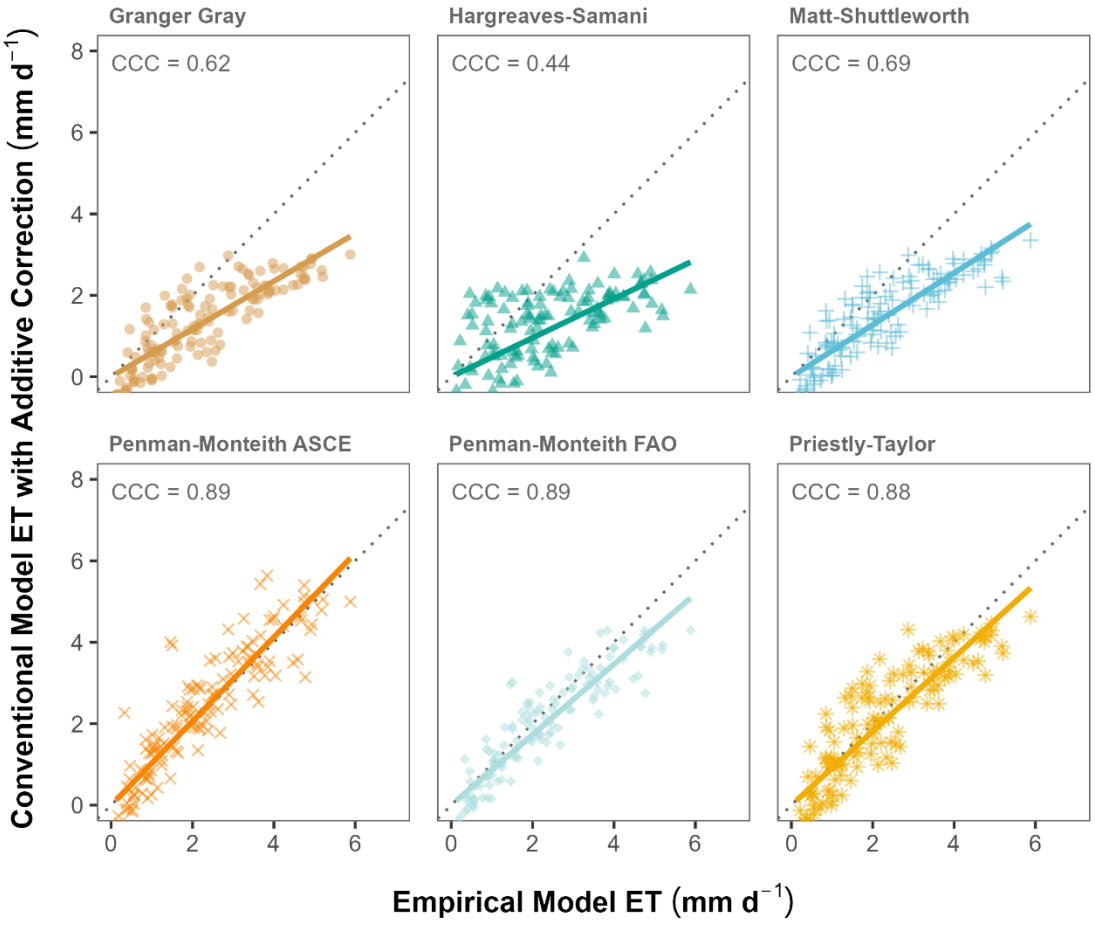

Figure S3: Daily ET calculated from our basin-scale, empirically-based model vs. ET from six conventional models modified with an additive correction factor. Dotted lines depict 1:1 relationships. CCC = concordance correlation coefficient.

Supplemental References

Achanta, R., Shaji, A., Smith, K., Lucchi, A., Fua, P., and Süsstrunk, S.: SLIC superpixels compared to state-of-the-art superpixel methods, IEEE Trans. Pattern Anal. Mach. Intell., 34, 2274–2282, https://doi.org/10.1109/TPAMI.2012.120, 2012.

Allen, R. G., Pereira, L. S., Raes, D., and Smith, M.: Crop evapotranspiration – Guidelines for computing crop water requirements, FAO Irrigation and Drainage Paper No. 56, FAO, Rome, 1998.

Allen, R. G.: The ASCE standardized reference evapotranspiration equation, ASCE/EWRI Task Committee Report, American Society of Civil Engineers, https://doi.org/10.1061/9780784408056, 2005.

Alonzo, M., Andersen, H. E., Morton, D. C., and Cook, B. D.: Quantifying boreal forest structure and composition using UAV structure from motion, Forests, 9, 119, https://doi.org/10.3390/f9030119, 2018.

Alonzo, M., Dial, R. J., Schulz, B. K., Andersen, H.-E., Lewis-Clark, E., Cook, B. D., and Morton, D. C.: Mapping tall shrub biomass in Alaska at landscape scale using structure-from-motion photogrammetry and lidar, Remote Sens. Environ., 245, 111841, https://doi.org/10.1016/j.rse.2020.111841, 2020.

Axelsson, P.: DEM generation from laser scanner data using adaptive TIN models, Int. Arch. Photogramm. Remote Sens. Spatial Inf. Sci., 33, 110–117, 2000.

Garcia, A., Johnson, M. J., Andraski, B. J., Halford, K. J., and Mayers, C. J.: Portable chamber measurements of evapotranspiration at the Amargosa Desert Research Site near Beatty, Nye County, Nevada, 2003–06, U.S. Geological Survey Scientific Investigations Report 2008–5135, Reston, VA, 2008.

Geoghegan, E. K., Caplan, J. S., Leech, F. N., Weber, P. E., Bauer, C. E., and Mozdzer, T. J.: Nitrogen enrichment alters carbon fluxes in a New England salt marsh, Ecosyst. Health Sustain., 4, 277–287, https://doi.org/10.1080/20964129.2018.1532772, 2018.

Granger, R. J. and Gray, D. M.: Evaporation from natural nonsaturated surfaces, J. Hydrol., 111, 21–29, https://doi.org/10.1016/0022-1694(89)90249-7, 1989.

Guo, D., Westra, S., and Maier, H. R.: An R package for modelling actual, potential and reference evapotranspiration, Environ. Model. Softw., 78, 216–224, https://doi.org/10.1016/j.envsoft.2015.12.019, 2016.

Hamel, P., McHugh, I., Coutts, A., Daly, E., Beringer, J., and Fletcher, T. D.: Automated chamber system to measure field evapotranspiration rates, J. Hydrol. Eng., 20, 04014037, https://doi.org/10.1061/(ASCE)HE.1943-5584.0001006, 2015.

Hargreaves, G. H. and Samani, Z. A.: Reference crop evapotranspiration from temperature, Appl. Eng. Agric., 1, 96–99, https://doi.org/10.13031/2013.26773, 1985.

Luo, C., Wang, Z., Sauer, T. J., Helmers, M. J., and Horton, R.: Portable canopy chamber measurements of evapotranspiration in corn, soybean, and reconstructed prairie, Agric. Water Manag., 198, 1–9, https://doi.org/10.1016/j.agwat.2017.11.024, 2018.

Norman, J. M., Kucharik, C. J., Gower, S. T., Baldocchi, D. D., Crill, P. M., Rayment, M., Savage, K., and Striegl, R. G.: A comparison of six methods for measuring soil-surface carbon dioxide fluxes, J. Geophys. Res.-Atmos., 102, 28771–28777, https://doi.org/10.1029/97JD01440, 1997.

Priestley, C. H. B. and Taylor, R. J.: On the assessment of surface heat flux and evaporation using large-scale parameters, Mon. Weather Rev., 100, 81–92, https://doi.org/10.1175/1520-0493(1972)100<0081:OTAOSH>2.3.CO;2, 1972.

Shuttleworth, W. J. and Wallace, J. S.: Evaporation from sparse crops – An energy combination theory, Q. J. R. Meteorol. Soc., 111, 839–855, https://doi.org/10.1002/qj.49711146910, 1985.